Journal of Power Sources 246 (2014) 457–463

Contents lists available at ScienceDirect

Journal of Power Sources

journal homepage: www.elsevier.com/locate/jpowsour

Sc-substituted $La_{0.6}Sr_{0.4}FeO_{3-\delta}$ mixed conducting oxides as promising electrodes for symmetrical solid oxide fuel cells

Xuejiao Liu, Da Han, Yucun Zhou, Xie Meng, Hao Wu, Junliang Li, Fanrong Zeng, Zhongliang Zhan*

CAS Key Laboratory of Materials for Energy Conversion, Shanghai Institute of Ceramics, Chinese Academy of Sciences (SICCAS), 1295 Dingxi Road, Shanghai 200050, China

HIGHLIGHTS

- $La_{0.6}Sr_{0.4}Fe_{0.9}Sc_{0.1}O_{3-\delta}$ oxides show good stability in both oxidizing and reducing environments.
- $La_{0.6}Sr_{0.4}Fe_{0.9}Sc_{0.1}O_{3-\delta}$ electrodes exhibit polarization resistances of 0.015 Ω cm^2 in air and 0.29 Ω cm^2 in H_2 at 800 °C.
- Maximum power densities of 0.56 W cm^{-2} are obtained at 800 °C for symmetrical $La_{0.6}Sr_{0.4}Fe_{0.9}Sc_{0.1}O_{3-\delta}$ electrode fuel cells.

ARTICLE INFO

Article history:
Received 14 June 2013
Received in revised form
25 July 2013
Accepted 29 July 2013
Available online 7 August 2013

Keywords:
Scandium-substituted lanthanum strontium ferrite
Impregnation
Nanostructure
Reduced-temperature solid oxide fuel cells
Strontium- and magnesium-doped lanthanum gallate

ABSTRACT

The main barrier to symmetrical solid oxide fuel cells (SOFCs), where the same catalytic materials are used simultaneously as the anodes and the cathodes, is to identify a redox-stable catalyst that exhibits superior catalytic activities for both fuel oxidation and oxygen reduction reactions. Here we report a Sc-substituted $La_{0.6}Sr_{0.4}FeO_{3-\delta}$ oxide, $La_{0.6}Sr_{0.4}Fe_{0.9}Sc_{0.1}O_{3-\delta}$, that shows great promise as a new symmetrical electrode material with good structural stability and reasonable conductivities in air and hydrogen. We further demonstrate that nano-scale $La_{0.6}Sr_{0.4}Fe_{0.9}Sc_{0.1}O_{3-\delta}$ catalysts impregnated into the porous $La_{0.9}Sr_{0.1}Ga_{0.8}Mg_{0.2}O_{3-\delta}$ backbones exhibit good catalytic activities for oxygen reduction and hydrogen oxidation reactions and thereby yield low polarization resistances, *e.g.*, 0.015 Ω cm^2 in air and 0.29 Ω cm^2 in hydrogen with appropriate current collection at 800 °C. Thin $La_{0.9}Sr_{0.1}Ga_{0.8}Mg_{0.2}O_{3-\delta}$ electrolyte fuel cells with such symmetrical $La_{0.6}Sr_{0.4}Fe_{0.9}Sc_{0.1}O_{3-\delta}$ catalysts showed maximum power densities of 0.56 and 0.32 W cm^{-2} when operating on 97% H_2–3% H_2O at 800 and 700 °C, respectively.

1. Introduction

The solid oxide fuel cell (SOFC) is a clean and efficient device to generate electricity via electrochemically oxidizing a gaseous fuel that is separate from an oxidant gas (typically air) by an oxide ion-conducting and gas-impermeable electrolyte [1]. The traditional SOFC materials include yttria-stabilized zirconia (YSZ) electrolytes, Ni-YSZ cermet anodes and lanthanum strontium manganite or ferrite cathodes. The state-of-the-art anode-supported, thin YSZ electrolyte fuel cells usually provide maximum power densities of ≥1 W cm^{-2} at 800 °C in hydrogen fuels [2]. Such a high operating temperature, as required to facilitate the oxide ion transport through the electrolyte, allows SOFCs to operate on non-hydrogen fuels such as natural gas, gasified coal gas and biogas [3,4]. However, the Ni-YSZ anodes suffer from deactivation caused by sulphur poisoning and coking formation when exposed to these hydrocarbon fuels [5]. Another disadvantage with the Ni-cermet anodes is their large volume change associated with Ni ↔ NiO phase transformation and the resulting poor stability in redox cycling that might occasionally occur during the long-term operation [6]. Furthermore, the common cathode materials such as $La_{0.8}Sr_{0.2}MnO_{3-\delta}$ (LSM) and $La_{0.6}Sr_{0.4}Co_{0.8}Fe_{0.2}O_{3-\delta}$ (LSCF) are vulnerable to decomposition with dramatically decreased oxygen partial pressures around the triple phase boundaries for fuel cells operating at relatively low voltages, which would result in redox degradation of the cathodes and thereby adversely influence the long-term stability of the fuel cell performance.

An effective approach to address the above practical issues is simultaneous use of a redox-stable catalyst as both the anode and

* Corresponding author. Tel./fax: +86 21 6998 7669.
E-mail address: zzhan@mail.sic.ac.cn (Z. Zhan).

0378-7753/$ – see front matter © 2013 Elsevier B.V. All rights reserved.
http://dx.doi.org/10.1016/j.jpowsour.2013.07.111

the cathode in the newly-developed symmetrical solid oxide fuel cells, where the catalytic activities of the deactivated anodes can be readily restored by oxidizing carbon deposits and/or sulphur-contaminants during the redox cycles [7]. The symmetrical SOFCs also bring about additional advantages such as simplified fabrication procedures and minimized compatibility issues. In order to function well as the anodes and cathodes concurrently, the symmetrical catalyst materials should exhibit good structural stability and high conductivities over a wide range of oxygen partial pressures of 10^{-20}–1 atm as well as reasonably high catalytic activities toward fuel oxidation and oxygen reduction reactions. Such demanding requirements seriously restricted the choice of symmetrical electrode materials, most of which were derived from the SOFC interconnect or oxide anode materials such as $La_{0.7}Ca_{0.3}CrO_{3-\delta}$ (LCC) [8,9], A- or B-site modified chromium manganites [7,10] and substituted strontium titanates [11]. Nevertheless, insufficient catalytic activities for fuel oxidation and oxygen reduction reactions necessitate a relatively high operating temperature, typically in excess of 850 °C. Incorporation of some noble metal catalysts such as Pt, Ag or Au into the symmetrical electrodes can enhance their catalytic activities, but might be problematic for practical applications due to their prohibitive costs [12]. Mixed-conducting doped ceria such as $Ce_{0.9}Gd_{0.1}O_{1.95}$ (GDC) was also introduced as the catalyst in some cases. Up to date, the best results were achieved with symmetrical fuel cells based upon nanostructured LCC–GDC electrodes that showed maximum power densities of 0.64 W cm^{-2} at 900 °C in hydrogen fuels [13].

An alternative approach to obtain symmetrical electrode materials is to modify the typical lanthanum strontium manganite or ferrite cathode materials via doping the B-site with Mo^{4+}, Cr^{3+} and Sc^{3+} that help to stabilize these perovskite oxides in the strong reducing atmospheres, such as $La_{0.6}Sr_{0.4}Fe_{0.9}Sc_{0.1}O_{3-\delta}$ [7], $SrFe_{0.75}Mo_{0.25}O_3$ (SFMO) [14], $La_{0.8}Sr_{0.2}Mn_{0.8}Sc_{0.2}O_3$ [15] and $La_{0.3}Sr_{0.7}Cr_{0.3}Fe_{0.7}O_3$ [16]. LSGM electrolyte supported fuel cells with symmetrical SFMO electrodes showed maximum power densities of 0.65 W cm^{-2} at 850 °C in hydrogen fuels [14]. Prior reports have shown that $La_{0.6}Sr_{0.4}Fe_{0.9}Sc_{0.1}O_{3-\delta}$ symmetric electrodes could only work well on YSZ or LSGM electrolytes at temperatures above 850 °C [7]. Here we investigate the stability of $La_{0.6}Sr_{0.4}Fe_{0.9}Sc_{0.1}O_{3-\delta}$ in both air and hydrogen atmospheres, and compare the catalytic activities for oxygen reduction and fuel oxidation reactions. Furthermore, we demonstrate that thin LSGM electrolyte fuel cells with nanostructured $La_{0.6}Sr_{0.4}Fe_{0.9}Sc_{0.1}O_{3-\delta}$ electrodes rendered power densities in hydrogen fuels as high as 0.56 and 0.32 W cm^{-2} at 800 and 700 °C, respectively.

2. Experimental

$La_{0.6}Sr_{0.4}Fe_{0.9}Sc_{0.1}O_{3-\delta}$ (LSFSc) powders were synthesized via a sol–gel combustion method. Stoichiometric amounts of analytical grade $La(NO_3)_3\cdot 6H_2O$, $Sr(NO_3)_2$, $Fe(NO_3)_3\cdot 9H_2O$ and $Sc(NO_3)_3\cdot 9H_2O$ were dissolved in deionized water. These nitrates were 99% pure and purchased from Sinopharm Chemical Reagent. Citric acid was adopted as the complexing agent and added in a 1:1 molar ratio of citric acid to the total metal ions while keeping continuous stirring with the pH value adjusted to ≈6 via addition of ammonia. The resulting solution was slowly heated on a hotplate until self-combustion occurred. The ash was pulverized and then calcinated at 950 °C for 4 h in air. For material structural stability tests, some of the powders were heat-treated in dry hydrogen at 800 °C for 10 h. The phase structures of powders as synthesized in air and those heat-treated in hydrogen were examined at room temperature using an X-ray diffractometer (XRD) (Rigaku-D-Max γA) with a scanning range of 20–80°. The as-synthesized $La_{0.6}Sr_{0.4}Fe_{0.9}Sc_{0.1}O_{3-\delta}$ powders were compacted into a cylinder with a diameter of 13 mm and then fired in air at 1350 °C. The electrical conductivities of LSFSc were measured in dry hydrogen and ambient air from 500 to 850 °C using a standard four-probe DC method.

Thin $La_{0.9}Sr_{0.1}Ga_{0.8}Mg_{0.2}O_{3-\delta}$ (LSGM) electrolyte SOFCs with symmetrical LSFSc electrodes were fabricated using a two-step procedure. Firstly, a tri-layer structure – porous|dense|porous LSGM – was fabricated by laminating three tape-cast ceramic green tapes with 40 wt% starch filler used as the fugitive material for the two porous layers, followed by co-firing at 1450 °C to densify the LSGM electrolyte layer. In the second step, LSFSc catalysts were coated on the internal surfaces of the two porous LSGM layers via the liquid impregnation technique as previously reported [17]. Specifically, nitrate solutions containing $La(NO_3)_3\cdot 6H_2O$, $Sr(NO_3)_2$, $Fe(NO_3)_3\cdot 9H_2O$, $Sc(NO_3)_3\cdot 9H_2O$ and citric acid in appropriate ratios were impregnated into the porous LSGM backbones and calcinated at 950 °C for 4 h. The ultimate loadings of the impregnated LSFSc catalysts in the porous LSGM layers were controlled by varying the number of impregnation/calcinations cycles. Note that additional impregnation of copper nitrate, after impregnation and calcination of LSFSc catalysts at 950 °C, was in some cases conducted with subsequent calcinations at 450 °C to form copper oxide. The cell structure was examined after testing using scanning electron microscopy (SEM) in a Hitachi S-4800-II microscope.

For electrochemical measurement, silver paste was applied on the electrode surfaces as the current collector. Current–voltage curves and electrochemical impedance spectra were obtained using an IM6 Electrochemical Workstation (ZAHNER, Germany) with one side exposed to ambient air and the other to humidified (3% H_2O) hydrogen at a flow rate of 100 mL min^{-1}. The individual electrode polarization resistances were determined by testing such symmetrical fuel cells in the single-chamber mode with humidified hydrogen for the anode and ambient air for the cathode, respectively.

3. Results and discussion

Fig. 1a shows the X-ray diffraction patterns of LSFSc powders calcinated at 950 °C in air, which can be refined using MDI Jade 6.0 software as a rhombohedral crystal structure and $R\bar{3}c$ space group with a = 5.5131 Å, α = 89.913°, and V = 167.57 Å^3. In order to examine the phase stability of LSFSc in the reducing atmosphere, these powders were heat-treated in dry hydrogen at 800 °C for 10 h with the XRD patterns shown in Fig. 1b. Despite a small peak at $2\theta = 32.3°$ that can be attributed to the minor impurity of $SrLaFeO_4$, the perovskite structure with a rhombohedral symmetry was well-maintained in the strong reducing environment while the lattice parameters changed to a = 5.5280 Å, α = 89.914°, and V = 168.93 Å^3. Such a slight increase in the unit cell volume of approximately 0.8% correlates with reduction of LSFSc oxides and

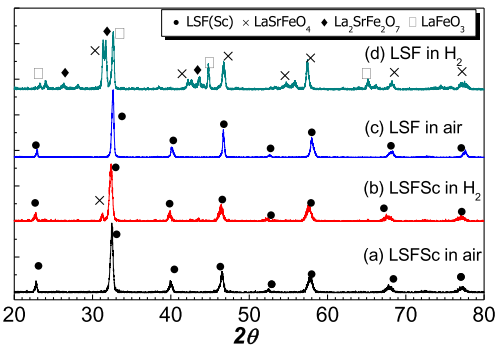

Fig. 1. X-ray diffraction patterns of $La_{0.6}Sr_{0.4}Fe_{0.9}Sc_{0.1}O_{3-\delta}$ (LSFSc) and $La_{0.6}Sr_{0.4}FeO_{3-\delta}$ (LSF) powders: (a) LSFSc calcinated in air at 850 °C, (b) LSFSc heat treated in H_2 at 800 °C, (c) LSF calcinated in air at 850 °C, (d) LSF heat treated in H_2 at 800 °C.

loss of some lattice oxygen as previously observed for $La_{0.75}Sr_{0.25}Cr_{0.5}Mn_{0.5}O_{3-\delta}$ (LSCM) [10]. Note that annealing longer than 10 h did not result in a pronounced increase in the diffraction peaks from the $SrLaFeO_4$ minor impurities. For comparison, the primitive $La_{0.6}Sr_{0.4}FeO_{3-\delta}$ oxide was prepared and heat-treated in the same manner, and X-ray diffraction patterns of the resulting powders (Fig. 1c and d) indicated that the rhombohedral perovskite structure as obtained in air was totally destroyed in dry hydrogen, producing a mixture of Fe, $LaSrFeO_4$, $La_2SrFe_2O_7$ and $LaFeO_3$. These results demonstrate that partial substitution of Sc for Fe in the B-site can substantially increase the chemical and structural stability of lanthanum strontium ferrite oxide against phase decomposition in reducing atmospheres, as previously observed for Sc-substituted $La_{0.8}Sr_{0.2}MnO_3$ [15].

Fig. 2 shows temperature dependence of the total electrical conductivities of LSFSc in air and hydrogen. In air, LSFSc exhibited a thermally activated semiconducting behaviour at low temperatures with the conductivity increasing with temperature. Nevertheless, the conductivity decreased above 650 °C with further increasing temperature, resulting from decreased charge carriers due to loss of lattice oxygen and the concomitant reduction of Fe^{4+} to Fe^{3+} to maintain charge neutrality. Such a phenomenon was typical for the perovskite-related mixed electronic and ionic conducting oxides [16,18]. As shown in the Arrhenius' plot, transition from semiconducting to metallic behaviour yielded a pronounced change in the activation energies for electron transport in LSFSc, *i.e.*, 0.11 eV in the temperature range 500–650 °C and 0.027 eV between 650 and 800 °C. Fig. 2a also shows that the total conductivity of LSFSc in air varied between 98 and 108 S cm^{-1} at 500–800 °C, smaller than for the parent $La_{0.6}Sr_{0.4}FeO_{3-\delta}$ oxide [19]. Similar reduction in the electrical conductivity with Sc^{3+} substitution has previously been observed for Sc^{3+}-substituted $La_{0.8}Sr_{0.2}MnO_{3-\delta}$, which can be explained by the interference of valence-constant Sc^{3+} in the B-site with electron conduction through the over-lapping B–O–B bonds via a Zerner double-exchange mechanism [20].

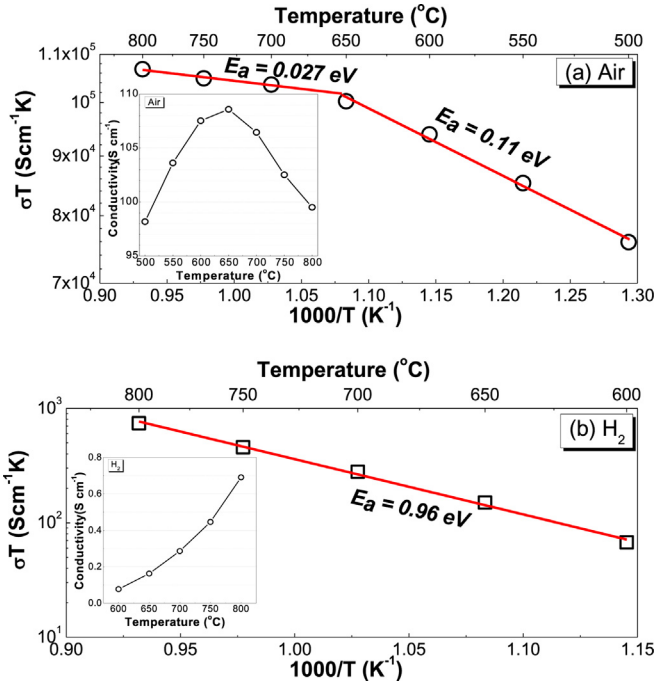

Fig. 2. The total electrical conductivities of $La_{0.6}Sr_{0.4}Fe_{0.9}Sc_{0.1}O_{3-\delta}$ in (a) dry air and (b) dry hydrogen.

Fig. 2b shows that the electrical conductivity of LSFSc in hydrogen increased from 0.077 S cm^{-1} at 600 °C monotonously to 0.69 S cm^{-1} at 800 °C. These values were almost two magnitudes smaller than for $SrFe_{1-x}Mo_xO_{3-\delta}$ [21], but much higher than the common redox-stable $La_{0.75}Sr_{0.25}Cr_{0.5}Mn_{0.5}O_{3-\delta}$ oxide [22]. Much lower conductivities of LSFSc in hydrogen than in air can be explained by the transition from a p-type conductor in oxidizing environments to an n-type conductor in reducing environments, where the main charge carriers were oxygen vacancies and electrons induced by losses of lattice oxygen. The activation energy for the total conductivity of LSFSc in dry H_2 was 0.96 eV over the temperature range of 600–800 °C that is between the values of ~0.7 eV for oxide-ion conduction and 2.2–2.4 eV for electronic conduction [19]. Increasing Sc^{3+} substitution to $x = 0.2$ did not eliminate the formation of $SrLaFeO_4$ minor impurities, but resulted in a large decrease in the conductivities, *e.g.*, 0.28 S cm^{-1} in H_2 (25 S cm^{-1} in air) at 800 °C. Therefore, higher Sc^{3+} substitution than $x = 0.1$ in $La_{0.6}Sr_{0.4}FeO_{3-\delta}$ was not further explored in this paper.

In order to examine the electrochemical behaviour of LSFSc as the symmetrical electrode material, symmetrical fuel cells were fabricated from an LSGM tri-layer – 18 μm thick dense layer sandwiched between two 200 μm thick porous layers, where LSFSc were simultaneously coated onto the internal surfaces of the porous LSGM backbones using the liquid impregnation technique that has shown great promise for formation of nano-scale catalysts with higher catalytic activities than the micron-scale catalysts [17,23]. Note that a volume loading of $V_{LSFSc} = 20\%$ was sufficient to form well-connected coatings on the pore walls (Fig. 3). Impedance measurements were performed on the symmetrical fuel cells in a uniform atmosphere of dry air or 97% H_2–3% H_2O to quantitatively determine the catalytic activities of the impregnated LSFSc–LSGM composite electrodes for oxygen reduction or hydrogen oxidation reactions, respectively. Silver paste was applied on the electrode surfaces as the current collector, and platinum paste was avoided so as to exclude its interference in evaluating catalytic properties of LSFSc catalysts for fuel oxidation and oxygen reduction reactions [24].

Fig. 4a shows the Nyquist plot of the EIS data in dry air at 800 °C that featured a small higher-frequency arc and a large lower-frequency arc with the summit frequency at ~500 Hz and ~5 Hz (Fig. 4c), respectively. With temperature decreasing to 700 °C, the lower-frequency arc remained almost unchanged while the higher-frequency arc increased exponentially and thereby became dominant, as shown in Fig. 4b. This is consistent with prior reports that the higher- and lower-frequency processes are related to oxygen-anion transfer from the deposited catalysts into the supporting backbones at their interfaces and the oxygen-exchange reaction on the catalyst surfaces [17], which dominate the oxygen reduction kinetics on the LSFSc impregnated LSGM cathodes at low and high temperatures, respectively. The overall cathode polarization resistances ($R_{P,C}$) correspond to the differences between the higher- and lower-frequency real-axis intercepts and are summarized in Fig. 4d. The $R_{P,C}$ value increased from 0.015 Ω cm^2 at 800 °C to 0.27 Ω cm^2 at 600 °C, much lower than for most symmetrical electrode materials currently under investigation. For example, LSCM–YSZ cathodes showed $R_{P,C}$ values of 0.09–0.27 Ω cm^2 on the YSZ electrolytes at 950–850 °C, whereas SFMO and $La_{0.75}Sr_{0.25}Cr_{0.5}Al_{0.5}O_{3-\delta}$ cathodes exhibited $R_{P,C}$ values of 0.24 Ω cm^2 at 780 °C and 0.18–1.2 Ω cm^2 at 950–800 °C on the LSGM electrolytes, respectively [7]. Fig. 4d also shows that the activation energy for oxygen reduction reactions on the impregnated LSFSc–LSGM cathodes was 1.18 eV.

Fig. 5a and b shows the Nyquist plots of the EIS data for the symmetrical fuel cells measured in 97% H_2–3% H_2O at 800 °C and 700 °C, respectively. Similar to oxygen reduction kinetics as

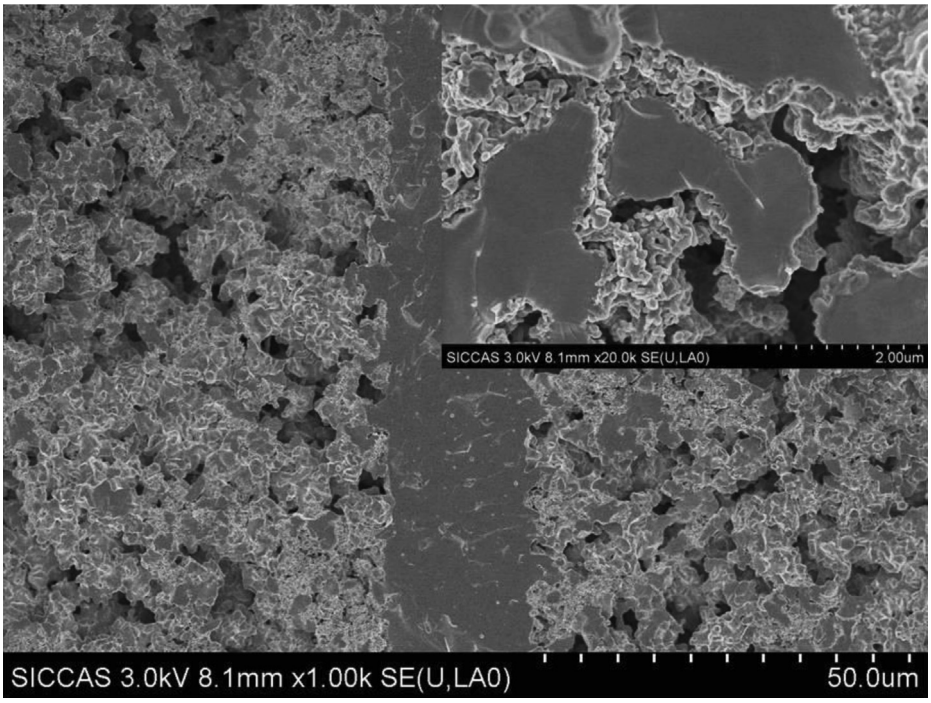

Fig. 3. SEM micrograph of the symmetrical fuel cell, LSFSc–LSGM|LSGM|LSGM–LSFSc. Inset is a higher magnification SEM image of the LSFSc coatings.

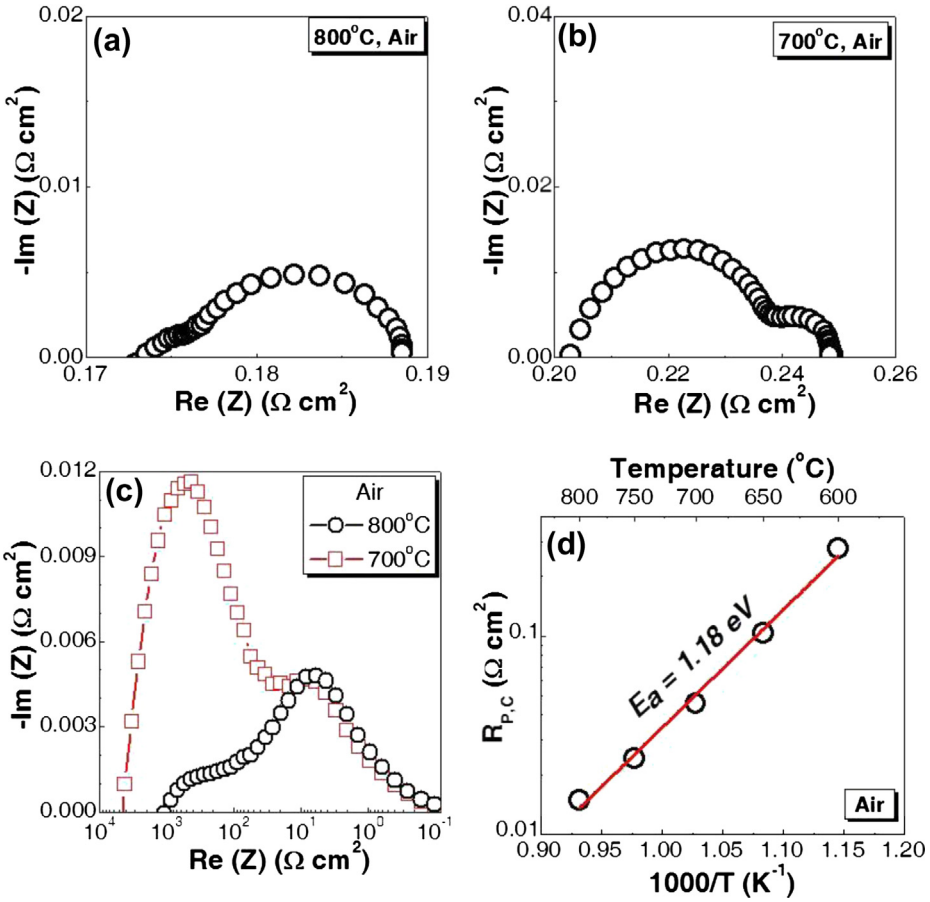

Fig. 4. Nyquist plots of the impedance data for symmetrical fuel cells, LSFSc–LSGM|LSGM|LSGM–LSFSc, measured in air at (a) 800 °C and (b) 700 °C. (c) Bode plots of (a) and (b). (d) The overall cathode polarization resistances plotted versus inverse temperature.

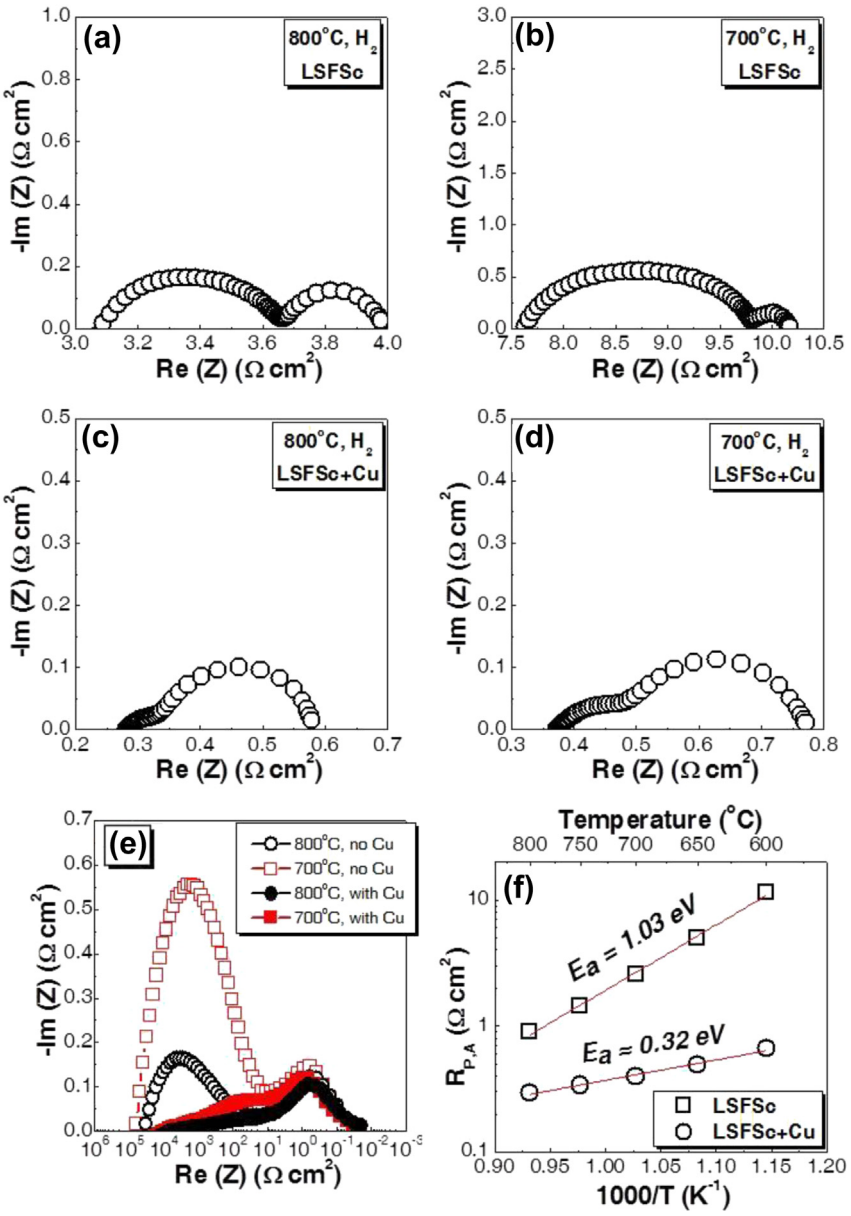

Fig. 5. Nyquist plots of the impedance data for symmetrical fuel cells LSFSc–LSGM|LSGM|LSGM–LSFSc, measured in hydrogen at (a, c) 800 °C and (b, d) 700 °C without (a, b) or with (c, d) copper addition. (e) Bode plots of (a–d). (f) The overall anode polarization resistances plotted versus inverse temperature.

discussed above, the higher-frequency arc increased substantially with decreasing temperature while the lower-frequency arc remained independent of temperature. The dominance of the higher-frequency arc at both temperatures seemingly indicated that oxygen-anion transfer from the supporting LSGM backbones to the deposited LSFSc catalysts along their interfaces was the rate-limiting step for hydrogen oxidation on the impregnated LSFSc–LSGM composite anodes. Nevertheless, concerns arise from the relatively low conductivities of LSFSc catalysts in the reducing atmospheres that might interfere with evaluation of their catalytic activities for hydrogen oxidation reactions, especially given the much larger ohmic resistances in hydrogen than in air, *e.g.*, 3.11 versus 0.174 Ω cm^2 at 800 °C as obtained from the higher-frequency real-axis intercepts in the Nyquist plots shown in Figs. 5a and 4a. Accordingly, additional impregnations of copper nitrate were conducted in some cases to provide enhanced current collection after calcinations at 450 °C in air and in-situ reduction during the measurement, as previously adopted for the Cu–CeO_2 co-impregnated YSZ composite anodes where copper was catalytically inert toward hydrogen oxidation reactions [4,25,26]. Such a low calcination temperature was used so as to prevent any chemical reaction between CuO and LSFSc perovskite oxides.

Fig. 5c and d shows the Nyquist plots of the EIS data for the symmetrical fuel cells with an additionally-deposited copper current collection layer measured in 97% H_2–3% H_2O at 800 °C and 700 °C, respectively. Notably, the presence of the copper layer resulted in a pronounced reduction of the pure ohmic resistance. For example, the ohmic resistance at 800 °C was 0.28 Ω cm^2 that, although still larger than observed in air shown in Fig. 4a, is approximately one order of magnitude smaller than the value of 3.11 Ω cm^2 shown in Fig. 5a for fuel cells without the copper layer. The most important observation is that the higher-frequency arc dropped dramatically with the introduction of the copper layer, *e.g.*, from 0.58 Ω cm^2 to 0.046 Ω cm^2 at 800 °C or from 2.19 Ω cm^2 to

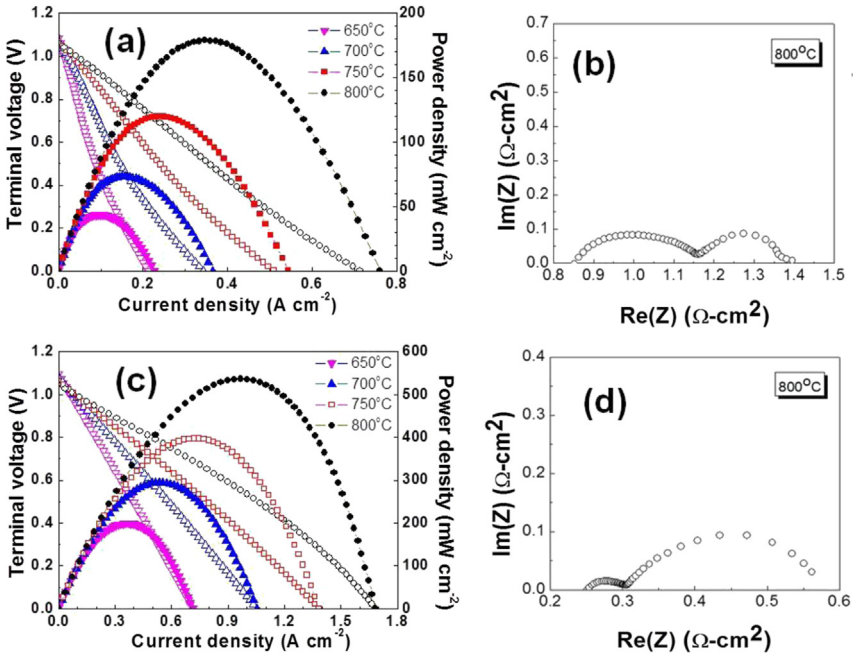

Fig. 6. Electrochemical characteristics of symmetrical fuel cells without (a, b) or with (c, d) copper current collection layer measured in humidified hydrogen fuel and dry air over the temperature range of 650–800 °C. All electrodes were ≈200 μm thick. (a, c) Plots of voltage and power density versus current density at 650–800 °C. (b, d) Representative impedance spectra measured at 800 °C and open circuits.

0.11 Ω cm^2 at 700 °C. These results indicate that quick electron transport, which was ensured by depositing a separate current collection layer in the present case, is critically important for facilitating oxygen anion transfer along the LSFSc|LSGM interfaces and thereby promoting hydrogen oxidation reactions. Another important observation is that the copper current collection layer did not alter the lower-frequency arc (Fig. 5e) that still remained in the range of 0.25–0.30 Ω cm^2 as observed in Fig. 5a–d. Much larger magnitude for the lower-frequency arc than for the higher-frequency arc (Fig. 5c and d) demonstrates the importance of tailoring the surface chemistry of the deposited catalysts to further promote surface gas exchange in enhancing their catalytic activities for hydrogen oxidation reactions.

Fig. 5f summarizes the anode polarization resistances ($R_{P,A}$) derived from the EIS data for the symmetrical fuel cells with or without the copper layer at varied temperatures. In the absence of the copper layer, the $R_{P,A}$ value increased from 0.89 Ω cm^2 at 800 °C to 11.39 Ω cm^2 at 600 °C, yielding an activation energy of 1.01 eV for hydrogen oxidation reactions on the impregnated LSFSc–LSGM composite anodes. On the other hand, the $R_{P,A}$ values were much smaller for the Cu and LSFSc co-impregnated LSGM composite anodes and varied between 0.28 Ω cm^2 at 800 °C and 0.63 Ω cm^2 at 600 °C. These values are comparable to those reported for the best-known SFMO electrode, and are much smaller than for other redox-stable anode materials such as 0.45 Ω cm^2 for $La_{0.3}Sr_{0.7}Fe_{0.8}Cr_{0.2}O_{3-\delta}$ at 750 °C, 0.35 Ω cm^2 for $La_{0.8}Sr_{0.2}Sc_{0.2}Mn_{0.8}O_{3-\delta}$ at 850 °C, 0.34 Ω cm^2 for LSCM–YSZ at 850 °C and 1.4 Ω cm^2 for $La_{0.7}Ca_{0.3}Cr_{0.5}Mn_{0.5}O_{3-\delta}$ at 800 °C [7]. Such low $R_{P,A}$ values for the present impregnated LSFSc–LSGM composites indicate that the LSFSc oxides, despite their low conductivities in hydrogen, exhibit superior catalytic activities for hydrogen oxidation reactions since prior reports have shown that the copper current collector is essentially inert [4,25,26]. Fig. 5f also shows that the presence of the copper layer resulted in a much smaller activation energy of 0.32 eV for hydrogen oxidation reactions, which results from increased dominance of surface gas exchange in the overall hydrogen oxidation kinetics that is much less temperature dependent.

Fuel cell measurement was also performed on the symmetrical fuel cells with one side exposed to dry air and the other to 97% H_2–3% H_2O. Again, some of these cells were impregnated with additional copper current collection layers in the anodes. Fig. 6a and c compares the typical polarization curves of cell voltages and

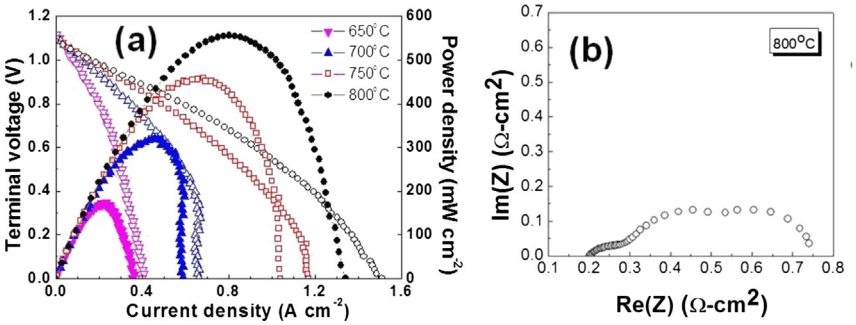

Fig. 7. (a) Voltage and power density versus current density for the symmetrical fuel cell with 40 μm thick anodes measured in humidified hydrogen fuel and dry air over the temperature range of 650–800 °C. (b) Representative impedance spectra measured at 800 °C and open circuits.

power densities as a function of current densities for the two types of fuel cells. For symmetrical fuel cells with no copper layer, the maximum power densities ranged between 0.18 W cm^{-2} at 800 °C and 0.044 W cm^{-2} at 650 °C. Such low power outputs were not unexpected and could be explained by large ohmic resistances and interfacial polarizations based upon impedance data (Fig. 6b), resulting primarily from poor conductivities of LSFSc catalysts in hydrogen as well as a relatively large anode thickness (*i.e.*, 200 μm). On the other hand, co-impregnation of a second copper layer dramatically increased the fuel cell power outputs with respective maximum power densities of 0.54, 0.40, 0.29 and 0.20 W cm^{-2} at 800, 750, 700 and 650 °C that were approximately 3–4 times as large as those obtained in the absence of copper layers. Such a pronounced enhancement was due to decreased ohmic resistances and anode polarizations with copper addition (Fig. 6d), as previously observed for ceria impregnated YSZ composite anodes [27].

An alternative approach to facilitate electron transport within the low-conductivity anodes is to reduce their thickness. Fuel cells with symmetrical LSFSc–LSGM electrodes were also fabricated from a different LSGM tri-layer – 18 μm thick dense layer sandwiched between 200 and 40 μm thick porous layers with LSFSc catalysts subsequently impregnated, where the thinner LSFSc–LSGM layers were used as the anode with no copper. Fig. 7a shows the typical polarization curves for the resulting symmetrical fuel cells. The maximum power densities were 0.56, 0.46, 0.32 and 0.17 W cm^{-2} at 800, 750, 700 and 650 °C, respectively. Comparison with results in Fig. 6a for fuel cells with 200 μm thick anodes demonstrates the effectiveness in enhancing the power densities via reducing low-conductivity anode thickness that yielded much smaller ohmic resistances and interfacial polarizations (Fig. 7b). The present results compare favourably with prior reports on SOFCs with impregnated oxide anode catalysts. For example, thin YSZ electrolyte fuel cells with LSCM impregnated YSZ anodes showed maximum power densities of 0.105 W cm^{-2} at 700 °C [24,27]. Such high power densities as obtained for symmetrical fuel cells with thin anodes in the absence of copper layer further confirmed that the LSFSc catalyst by itself has a superior catalytic activity for hydrogen oxidation reactions.

4. Conclusions

In summary, we have shown the great promise of the mixed-conducting LSFSc symmetrical electrode material with good structural stability and reasonable conductivities in air and hydrogen. Nano-scale LSFSc catalysts impregnated into the porous LSGM backbones exhibited high catalytic activities for oxygen reduction and hydrogen oxidation reactions and thereby yielded low polarization resistances, *e.g.*, 0.015 Ω cm^2 in air and 0.29 Ω cm^2 in hydrogen under the condition of quick electron transport at 800 °C. Thin LSGM electrolyte fuel cells with symmetrical LSFSc catalysts showed maximum power densities of 0.56 and 0.32 W cm^{-2} when operating on 97% H_2–3% H_2O at 800 and 700 °C, respectively.

Acknowledgements

The authors gratefully acknowledge the financial support of the National Basic Research Program of China under contract No. 2012CB215400, the National Science Foundation of China under contract No. 51072219, Science and Technology Commission of Shanghai Municipality under contract No. 11PJ1410300, Chinese Government High Tech Developing Project under contract No. 2011AA050702, and the 100 Talents Program of Chinese Academy of Sciences.

References

[1] A.J. Jacobson, Chem. Mater. 22 (2010) 660–674.
[2] S. de Souza, S.J. Visco, L.C. DeJonghe, J. Electrochem. Soc. 144 (1997) L35–L37.
[3] M. Mogensen, K. Kammer, Annu. Rev. Mater. Res. 33 (2003) 321–331.
[4] S. McIntosh, R.J. Gorte, Chem. Rev. 104 (2004) 4845–4865.
[5] A. Atkinson, S. Barnett, R.J. Gorte, J.T.S. Irvine, A.J. Mcevoy, M. Mogensen, S.C. Singhal, J. Vohs, Nat. Mater. 3 (2004) 17–27.
[6] T. Klemenso, M. Mogensen, J. Am. Ceram. Soc. 90 (2007) 3582–3588.
[7] J.C. Ruiz-Morales, D. Marrero-Lopez, J. Canales-Vazquez, J.T.S. Irvine, RSC Adv. 1 (2011) 1403–1414.
[8] N.Q. Minh, J. Am. Ceram. Soc. 76 (1993) 563–588.
[9] J.C. Ruiz-Morales, H. Lincke, D. Marrero-Lopez, J. Canales-Vazquez, P. Nunez, Bol. Soc. Esp. Ceram. V 46 (2007) 218–223.
[10] D.M. Bastidas, S.W. Tao, J.T.S. Irvine, J. Mater. Chem. 16 (2006) 1603–1605.
[11] J. Canales-Vazquez, J.C. Ruiz-Morales, D. Marrero-Lopez, J. Pena-Martinez, P. Nunez, P. Gomez-Romero, J. Power Sources 171 (2007) 552–557.
[12] J.C. Ruiz-Morales, J. Canales-Vazquez, D. Marrero-Lopez, D. Perez-Coll, J. Penia-Martinez, P. Nunez, J. Power Sources 177 (2008) 154–160.
[13] Y.C. Zhang, Y. Shen, X.B. Du, J.X. Li, X.J. Cao, T.M. He, Int. J. Hydrogen Energy 36 (2011) 3673–3680.
[14] Q.A. Liu, X.H. Dong, G.L. Xiao, F. Zhao, F.L. Chen, Adv. Mater. 22 (2010) 5478–5482.
[15] Y. Zheng, C. Zhang, R. Ran, R. Cai, Z.P. Shao, D. Farrusseng, Acta Mater. 57 (2009) 1165–1175.
[16] M. Chen, S. Paulson, V. Thangadurai, V. Briss, ECS Trans 45 (2012) 343–348.
[17] D. Han, X.J. Liu, F.R. Zeng, J.Q. Qian, T.Z. Wu, Z.L. Zhan, Sci. Rep. UK 2 (2012).
[18] G.L. Xiao, Q. Liu, S.W. Wang, V.G. Komvokis, M.D. Amiridis, A. Heyden, S.G. Ma, F.L. Chen, J. Power Sources 202 (2012) 63–69.
[19] M.V. Patrakeev, J.A. Bahteeva, E.B. Mitberg, I.A. Leonidov, V.L. Kozhevnikov, K.R. Poeppelmeier, J. Solid State Chem. 172 (2003) 219–231.
[20] H.X. Gu, Y. Zheng, R. Ran, Z.P. Shao, W.Q. Jin, N.P. Xu, J. Ahn, J. Power Sources 183 (2008) 471–478.
[21] G.L. Xiao, Q. Liu, X.H. Dong, K. Huang, F.L. Chen, J. Power Sources 195 (2010) 8071–8074.
[22] S.W. Tao, J.T.S. Irvine, J. Electrochem. Soc. 151 (2004) A252–A259.
[23] Z.L. Zhan, D. Han, T.Z. Wu, X.F. Ye, S.R. Wang, T.L. Wen, S. Cho, S.A. Barnett, RSC Adv. 2 (2012) 4075–4078.
[24] G. Kim, S. Lee, J.Y. Shin, G. Corre, J.T.S. Irvine, J.M. Vohs, R.J. Gorte, Electrochem. Solid-State Lett. 12 (2009) B48–B52.
[25] S.D. Park, J.M. Vohs, R.J. Gorte, Nature 404 (2000) 265–267.
[26] S.W. Jung, C. Lu, H.P. He, K.Y. Ahn, R.J. Gorte, J.M. Vohs, J. Power Sources 154 (2006) 42–50.
[27] M.D. Gross, J.M. Vohs, R.J. Gorte, J. Electrochem. Soc. 154 (2007) B694–B699.